RSC Advances

PAPER

View Article Online
View Journal | View Issue

Cite this: *RSC Adv.*, 2021, **11**, 28052

β-Cyclodextrin functionalized 3D reduced graphene oxide composite-based electrochemical sensor for the sensitive detection of dopamine†

Xuan Chen,[a] Na Li,[a] Yanqin Rong,[c] Yuli Hou,*[b] Yu Huang[c] and Wenting Liang *[c]

A three-dimensional reduced graphene oxide nanomaterial with β-cyclodextrin modified glassy carbon electrode (3D-rGO/β-CD/GCE) was constructed and used to detect the electrochemical behavior of dopamine (DA). The nanocomposite materials were characterized by scanning electron microscopy (SEM), infrared spectrometry (FT-IR), Raman spectrogram and thermogravimetric analysis (TGA), which showed that β-CD was well modified on 3D graphene with a porous structure. The electrochemical properties of different modified electrodes were investigated by cyclic voltammetry (CV) and electrochemical impedance spectroscopy (EIS), proving the highest electron transfer rate of the 3D-rGO/β-CD modified electrode. The experimental conditions such as scan rate, pH, enrichment time and layer thickness were optimized. Under the best experimental conditions, DA was detected by differential pulse voltammetry (DPV) by 3D-rGO/β-CD/GCE with excellent electrocatalytic ability and satisfactory recognition ability, resulting in a wide linear range of 0.5–100 μM and a low detection limit (LOD) of 0.013 μM. The modified electrode based on 3D-rGO/β-CD nanocomposites is promising in the field of electrochemical sensors due to its high sensitivity and other excellent properties.

Received 23rd March 2021
Accepted 6th August 2021

DOI: 10.1039/d1ra02313f

rsc.li/rsc-advances

Introduction

Dopamine (DA), a crucial neurotransmitter, is responsible for the function of cardiovascular, central nervous, renal, and hormonal systems.[1,2] However, excess or insufficient concentrations of DA in nervous systems lead to schizophrenia, Parkinson's disease, hyperactive disorder, and so on,[3,4] so regular testing of dopamine levels in bodies of patients is required. Hence, it is especially significant for detecting DA molecules in the medical and biological field *via* a sensitive and effective assay.

At present, there are many classic strategies to detect DA including fluorescence spectrometry,[5] mass spectroscopy,[6] high performance liquid chromatography,[7] electrochemistry method[8–12] and so on. Considering the relatively low content of DA in serum, the electrochemical approach is regarded as the effective one on account of high sensitivity apart from the other numerous advantages including facile operation, rapid detection and low cost. Nevertheless, conventional electrochemical sensors suffer from some restrictions as far as sensitivity and electron transfer ability are concerned using the bare GCE or carbon electrodes. To address these drawbacks, a variety of materials were fabricated to be modified on the surface of electrodes for enhancing the electrochemical performance in the detection of DA, such as carbon materials,[9–11] ionic conducting solid materials,[8] polymers,[12] metals or metal alloy and metal oxides.[13–15] Unfortunately, further limitations have been imposed on achieving wide detection range and low detection limit.

Compared with other materials, graphene-based nanomaterials exhibit their superiority such as large surface area and excellent conductivity, which are widely for the electrochemical biosensor.[16,17] Nevertheless, there still are some shortcomings in view of not the achievement of excellent water solubility and high selectivity as well as highly stable, which impede the great electrochemical application promise. Cyclodextrins (CDs), delightfully, have frequently acted as the water-soluble unit for functionalization of carbon materials, revealing the remarkable electrochemical performance by supramolecular recognizability and excellent capability of forming inclusion complexes with various guest molecules.[18–21] Currently, rGO–β-CD nanocomposite is one of the most widely used devices to detect many biomolecule analytes by the integration of the unique properties of graphene and β-CD, which extends individual performances of such two materials. For example, Heydari' group successfully achieved polymerization of water-insoluble β-cyclodextrin (β-CD)/graphene or graphene oxide using citric acid crosslinker, which was applied for detection of dopamine,

[a]*Department of Neurology, Taiyuan Central Hospital of Shanxi Medical University, Taiyuan 030062, China*

[b]*Department of Neurology, First Hospital of Shanxi Medical University, Taiyuan 030001, China. E-mail: houyuli2008@163.com*

[c]*Institute of Environmental Science, Shanxi University, Taiyuan 030006, China. E-mail: liangwt@sxu.edu.cn*

† Electronic supplementary information (ESI) available: EDS of 3D-rGO/β-CD; the cartograms of storage stability, repeatability and reproducibility of the 3D-rGO/β-CD/GCE sensor; determination of DA in human serum samples. See DOI: 10.1039/d1ra02313f

tyrosine and uric acid.[21] Likewise, a sensitive electrochemical sensor was also fabricated by Mirzaei *et al.* based on β-CD–rGO nanocomposite for measuring the curcumin. Unfortunately, the inevitable agglomeration of graphene nanosheets in an aqueous medium could obviously reduce the electrochemically active surface area, bringing about forming the relatively poor electrochemical behaviors thus fading the overall performances of designed sensors.[22] It necessitates the development of new composite to efficiently tackle the aforesaid issues.

Three-dimensional (3D) graphene derived from two-dimensional (2D) graphene assemblies, may be an excellent alternative served as an emerging functional material in the field of graphene chemistry. Moreover, the 3D porous graphene retains the intrinsic structure and characteristics of graphene, more importantly, also avoids the aggregation successfully due to in-plane pores and 3D cross-linking, which exhibits more outstanding merits including unique porous network structure, higher specific surface-area, better mechanical stability, higher catalytical activity, more remarkable conductivity and improved electron transfer ability, unfolding great potentials for electrochemical sensing.[10,23–26]

Hence, our present work is aimed at employing 3D-rGO as an electrode substrate for β-CD to create a new type of biosensor of 3D-rGO/β-CD based on host–guest interactions, which are applied for the sensitive and selective electrochemical measuring of DA, as shown in Scheme 1. The as-obtained 3D-rGO/β-CD effectively combined the exceptional electronic conductivity of 3D-rGO and gathering ability towards DA on the surface of β-CD with satisfactory recognition and improved the dispersibility and solubility, thus producing the significant synergistic effect to further enhance the electrochemical sensing signal and expand the detection range. Furthermore, this sensor was also applied for the detection in human serum with satisfactory results.

Experimental section

Materials

Graphite powder and β-cyclodextrin (β-CD) were purchased by Shanghai Macklin Biochemical Technology Co. Ltd. Ammonia solution were purchased from Tianjin Hengxing Chemical Reagent Factory. 4-Dimethylaminopyridine (DMAP), 1-(3-dimethylaminopropyl)-3-ethylcarbodiimide hydrochloride (EDC·HCl) and dopamine (DA) were produced by Aladdin Industrial Corporation of Shanghai. Except that the purity of ammonia water is 25%, other available reagents were of analytical grade without further purification. All solutions were prepared *via* ultra-pure water purified with the Millipore system from USA.

Instruments

All the electrochemical tests were performed on CHI660E electrochemical workstation (Shanghai Chenhua Instruments Co., China) using the standard three electrode system. The bare GCE or modified GCE electrode (3.0 mm) were used as the working electrode, the saturated calomel electrode as the reference electrode and the platinum wire electrode as the auxiliary electrode. Scanning Electron Microscopy (SEM) images were obtained by scanning electron microscope of S-4800 (Hitachi, Japan). Energy-dispersive X-ray spectrometry (EDS) recorded on Oxford Instruments X-Max N is to analyse elements of the as-fabricated samples. Fourier transform infrared (FT-IR) spectrogram and thermogravimetric analysis (TGA) data was respectively obtained on a Bruker Tensor and TA Instruments Q50 in the presence of nitrogen flow. UV spectra were measured *via* a Lambda 950 UV-vis spectrophotometer from Perkin Elmer. Raman spectroscopy was performed on LabRAM HR of Horiba. Contact angles were measured on a drop shape analysis system KRUSS/DSA25 contact angle system.

Synthesis of 3D-rGO/β-CD

According to our previous reported literature, 3D-rGO was in advance obtained by the reduction of GO using the L-Cys as reducing agent.[10,23] Then 20 mg 3D-rGO powder was dissolved in the ultra-pure water/DMSO (4 : 1) under the ultrasound to form uniform dispersion solution and with the addition of 1-(3-dimethylaminopropyl)-3-ethylcarbodiimide hydrochloride (EDC·HCl, 23 mg, 0.12 mmol) and 4-dimethylaminopyridine (DMAP, 14.7 mg, 0.12 mmol) to activate the surface of carboxylic groups from 3D-rGO for 2 h. After that, 400 mg β-CD powder was added to the above mixture for keeping stirring 24 h at room temperature. The as-prepared 3D-rGO/β-CD were washed with ultrapure water several times and finally dried at 60 °C for 24 h to yield the black power.

Fabrication of the 3D-rGO/β-CD modified GCE

Firstly, the bare GCE (diameter: 3 mm) was polished by alumina slurry with various sizes (1.0, 0.3, 0.05 μm) in turn, and washed with ethanol and ultrapure water under ultrasonic conditions, then dried in air at room temperature. Secondly, the dispersion of

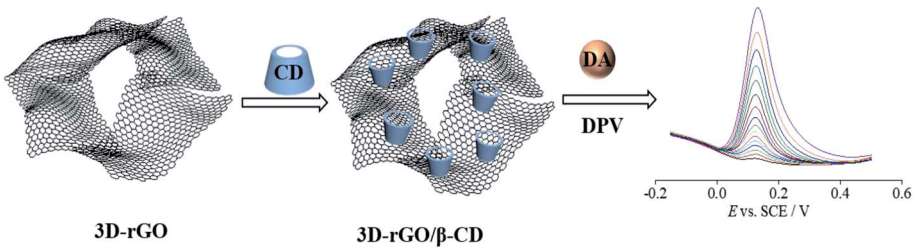

Scheme 1 Illustration of the procedure for preparing 3D-rGO/β-CD, and sensing the dopamine by an electrochemical strategy.

3D-rGO/β-CD was obtained by adding 3D-rGO/β-CD power of 1 mg into 0.5 mL mixture of ethanol and water containing Nafion followed by ultrasonication for several minutes. Finally, 6 μL dispersion was drop-cast slowly onto the surface of cleaned GCE and dried naturally to get the 3D-rGO/β-CD/GCE for further use.

Electrochemical studies

3D-rGO/β-CD modified GCE were characterized by electrochemical impedance spectroscopy (EIS) and cyclic voltammograms (CV) in the pH phosphate buffer (0.1 M PB) of 7.0 containing 5 mM $[Fe(CN)_6]^{3-/4-}$ and 0.1 M KCl. EIS experiments were recorded at a potential of 0.188 V over the frequency range from 10 mHz to 100 kHz, using an amplitude of 5 mV. CV data were performed in the DA solution of PB in the potential range from −0.2 V to 0.6 V at a scan rate of 0.1 V s^{-1}. Electrochemical measurements of DA by differential pulse voltammetry (DPV) were recorded in 0.1 M PB of pH 7.0 containing DA. Additionally, 3D-rGO/β-CD/GCE was also applied in serum for practical sample detection.

Real sample analysis

The 3D-rGO/β-CD modified electrode was applied to detect DA from human serum and urine (both provided by Taiyuan Central Hospital of Shanxi Medical University) to evaluate the accuracy and applicability. Briefly, for human serum sample, fresh blood was collected in clean plastic tubes, and interfering proteins in pristine serum removed by centrifugation at 8000 rpm for several minutes to extract the supernatant as serum. Next, the serum samples were diluted 5-fold with 0.1 M phosphate buffer (PB) solution (pH = 7.0) before determination. For urine sample, the human urine was diluted 2 times for the detected DA concentration which was in the linear range according to the calibration curves of DA. Then, the unknown concentration of dopamine was predetermined by DPV to obtain the original amount DA in serum and urine. After that, by adding the known quantity of different standard DA concentration into the diluted serum and urine to get five samples, the accuracy experiments for dopamine detection in human serum and urine samples were performed with the standard addition method by determining the recovery of dopamine.

Results and discussion

Characterization of 3D-rGO/β-CD

SEM was used to observe surface morphology of 3D-rGO/β-CD nanocomposites. From the SEM images of two different magnifications in Fig. 1(a) and (b), it can be seen that randomly oriented rGO sheets stack, twist and wrap to form a three-dimensional porous and fully connected framework, meanwhile, the modification of β-CD does not affect the network structure of reduced graphene oxide. In addition, EDS spectra of 3D-rGO/β-CD contains peaks of C and O even N and S elements (Fig. S1†), which confirms the unavoidable doping of S and N atoms in the synthetic process of 3D-rGO.

FI-IR spectroscopy is an important method to analyze the surface structure of as-prepared composites. Fig. 2 describes the FT-IR spectrograms of β-CD, 3D-rGO and 3D-rGO/β-CD. In the β-CD curve, 3400 cm^{-1} and 2928 cm^{-1} respectively represent the stretching vibration absorption peak of O–H and CH_2 (methylene). Additionally, the characteristic absorption bands in the range from 1155 to 1030 cm^{-1} are ascribed to the saccharide structure from β-CD. Detailedly, the significant peaks at 1155 cm^{-1} refers to antisymmetric glycosidic C–O–C stretching/O–H bending vibrations, and the coupled C–O/C–C stretching/O–H bending vibration of β-CD are located at 1030 and 1076 cm^{-1}.[21] For 3D-rGO, the peaks at 1558 cm^{-1} and 1190 cm^{-1} belong to the stretching vibration of C=C and C–C/C–N, respectively.[27] Meanwhile, several peaks at 2928 cm^{-1}, 1716 cm^{-1} and 1402 cm^{-1} may be associated with the stretching vibration of the aromatic C–H, C=O and C–OH, respectively.[28] In case of 3D-rGO/β-CD, it can be observed that the peak at 2928 cm^{-1} is weaken to a large extent relative to β-CD, and the region of 1155 to 1030 cm^{-1} combines the featured absorption band of cyclodextrin and the C–C/C–N stretching vibration peak of 3D-rGO, giving rise to the changes in the intensity without the approximately obvious peak shifts. Moreover, as clearly seen, 3D-rGO/β-CD exhibits the shift of peak from 1715 cm^{-1} of 3D-rGO to 1716 cm^{-1} attributed to C=O of ester bond, which originates from the reaction between COOH groups of 3D-rGO and OH groups of β-CD, further certifying that the β-CD has been successfully settled on the surface of 3D-rGO.

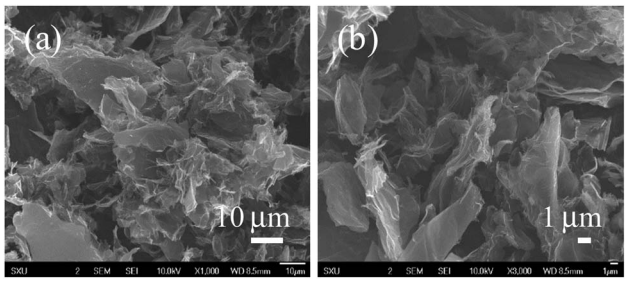

Fig. 1 SEM images at different magnifications (a) and (b) of 3D-rGO/β-CD.

The structural analysis and electronic properties of graphene-based materials were further elucidated by Raman spectroscopy. From Fig. 3(a), 3D-rGO sheets and 3D-rGO/β-CD exhibits the carbonaceous D bands at 1350 cm^{-1} and G band located at 1580 cm^{-1}, which represents the disorder and defects

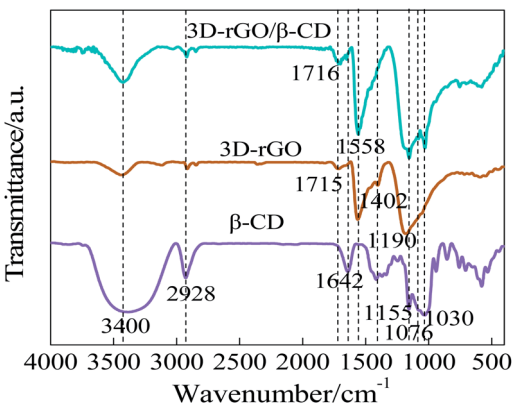

Fig. 2 FT-IR spectrogram of β-CD, 3D-rGO and 3D-rGO/β-CD.

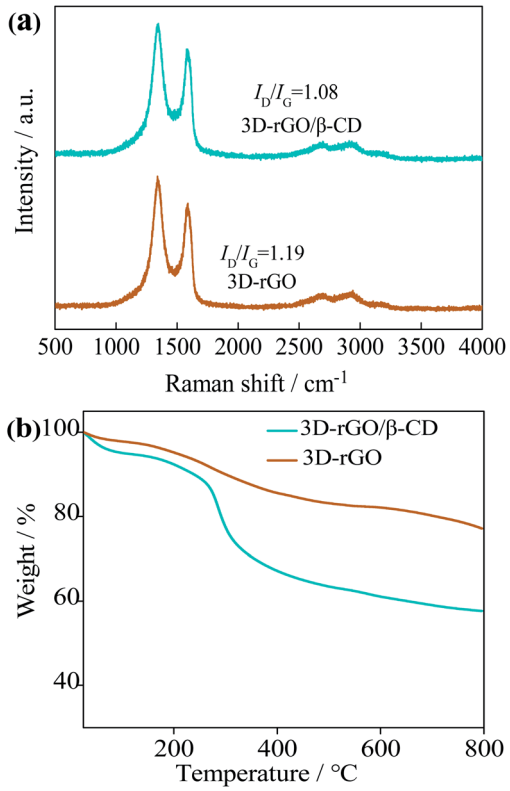

Fig. 3 (a) Raman spectrogram of 3D-rGO and 3D-rGO/β-CD; (b) thermogravimetric analysis of 3D-rGO and 3D-rGO/β-CD.

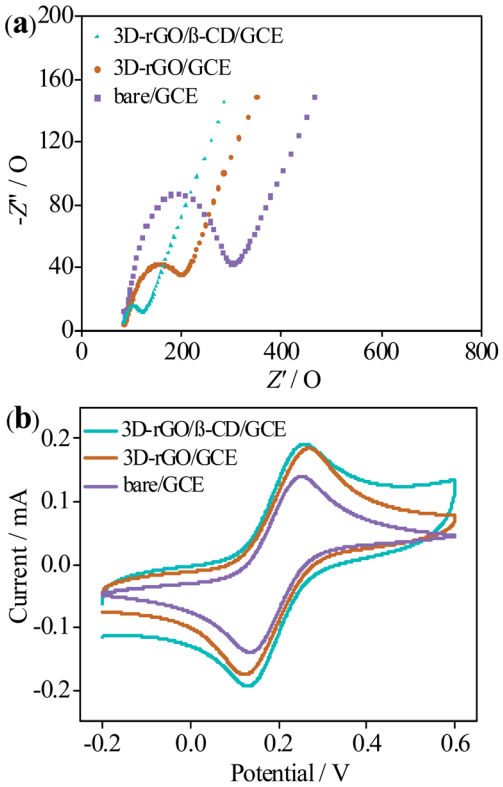

Fig. 4 Nyquist curves (a) and cyclic voltammograms (b) of bare GCE, 3D-rGO and 3D-rGO/β-CD modified GCE in a 10.0 mL 0.1 M PB containing 5 mM $[Fe(CN)_6]^{3-/4-}$ and 0.1 M KCl (pH 7.0).

in the hexagonal graphitic layers and E_{2g} mode of ordered sp^2 hexagonal carbon, respectively.[29] In general, the ratio of D/G band intensity (I_D/I_G) is expected to quantify the degree of disorder, and the I_D/I_G ratio of 3D-rGO is found to be 1.19, which is higher than the value of GO (0.92) in previous literature.[10] It is caused by the increase of carbon cavities and disorder degree in the process of reduction of GO and the synthesis of 3D framework. For the 3D-rGO/β-CD curve, I_D/I_G ratio of the composite is decreased to 1.08. In comparison to 3D-rGO, the lower I_D/I_G value of 3D-rGO/β-CD confirms that the modification of β-CD onto the 3D network of rGO resulted in the reduced numbers of defect.

TGA data, displayed in Fig. 3(b), depicts the β-CD content carried by 3D-rGO. Here, it is visible that 3D-rGO/β-CD nanocomposites show the three-step degradation throughout the temperature-rising process. In the first degradation step, before 280 °C, it may be due to the evaporation of water and oxygen containing groups. The second strong mass loss could be explained by the decomposition of β-CD from 280 °C to 400 °C. When the temperature rises between 400 °C and 800 °C, the weight reduction is distinctly slight, which is possibly a small amount of collapse for 3D-rGO/β-CD framework. In comparison, no evidently major weight loss for the 3D-rGO is observed, proving the good thermal stability. According the calculation results, it is concluded that 3D-rGO combines with about 17 wt% β-CD.

Electrochemical characterization of 3D-rGO/β-CD/GCE

EIS and CV are frequently assessed the electron transfer capability of modified GCEs by nanomaterials. As shown in Fig. 4a, the impedance curve includes half circle in the high frequency region and straight line in the low frequency region respectively corresponding to the electron transfer impedance (R_{et}) of modified layer between electrolyte and electrode and the diffusion resistance of the electrolyte on the modified layer surface. The Randles equivalent circuit model is used to fit EIS data (inset of Fig. 4a), where R_s is the uncompensated electrolyte resistance, Z_W represents the Warburg impedance.[8] By fitting the EIS data, the electron transfer resistance of each electrode is: bare GCE (270 Ω) > 3D-rGO/GCE (94.3 Ω) > 3D-rGO/β-CD/GCE (32.8 Ω), and the corresponding relative standard deviation (RSD) is 1.9% for bare GCE, 2.1% for 3D-rGO/GCE and 2.8% for 3D-rGO/β-CD/GCE. Compared with the R_{et} values, it is obvious that the impedance of the bare electrode is the largest, illustrating that the electron transfer ability of the bare electrode is the worst. The semicircle diameter of 3D-rGO/β-CD/GCE is significantly smaller than that of 3D-rGO/GCE. The small impedance of 3D-rGO/β-CD gives the credit to the excellent water solubility of β-CD and the outstanding electrical conductivity of 3D-rGO, which makes the dispersion of nanomaterials on the electrode more uniform, resulting the electronic transfer of 3D-rGO/β-CD/GCE at the interface is easier by synergistic effect.

At the same time, CV measurements were performed for different electrodes in PB solution (pH = 7) of 0.1 M KCl, using $[Fe(CN)_6]^{3-/4-}$ as redox probe. From Fig. 4b, high peak current of 3D-rGO/β-CD/GCE is observed in contrast to the else two

electrodes. This phenomenon is not only attributed to the outstanding conductivity of 3D-rGO, but also β-CD acted as an ideally water-soluble modification layer of 3D-rGO to enhance the dispersibility of 3D-rGO on the working electrode, thus improving the conductivity of 3D-rGO. Indeed, it is due to synergistic effect of 3D-rGO and β-CD that the electronic transfer of 3D-rGO/β-CD is accelerated, bringing about the high electrochemical performance, which is in agreement with the obtained results of impedance. Additional evidence for the enhanced solubility and dispersibility of 3D-rGO/β-CD by carrying β-CD onto 3D-rGO was provided by the contact-angle measurements.

The contact angles for water of GO, 3D-rGO and 3D-rGO/β-CD film were measured to be 78°, 83.5° and 70°, respectively (Fig. S2a, 2b and 2c†). Among three material films, 3D-rGO displays relatively strong hydrophobic interface with the highest contact angle due to the reduction of the hydrophilic oxygen-containing groups from GO. The smaller contact angle of the 3D-rGO/β-CD film relative to 3D-rGO manifestes its weaker hydrophobic, which is explained by the hydrophilic groups of the water-soluble β-CD molecules.

Likewise, considering the molecule DA with two hydroxyl groups, it may undergo a redox reaction process on the surface of electrodes. Fig. S3† displays the CVs results of DA on the bare/GCE, 3D-rGO/GCE, and 3D-rGO/β-CD/GCE, respectively. A pair of redox peaks are observed ranging from −0.2 V to 0.6 V of potential at bare GCE and modified GCEs, which were likely that phenolic hydroxyl group of DA was the oxidized into dopamine-*o*-quinone and reduced back to DA.[30] In Fig. S3,† for 3D-rGO/GCE, the improved peak intensity of DA compared to bare/GCE, is based on the introduction of 3D-rGO as an outstanding conductive 3D material, which can quicken the electron transfer of DA molecules between the surface of electrode and electrolyte. When β-CD were settled into the 3D-rGO nanosheets, the peaks of DA can be further increased relative to 3D-rGO, and the anodic peak current value (i_{pa}) of DA on the 3D-rGO/β-CD/GCE was about 3.67 times than that at bare/GCE, meaning the high sensitivity to DA of 3D-rGO/β-CD. In view of this improvement in the electrochemical response signal, one possible reason is that the enhancement of the concentration of DA molecules on the surface of 3D-rGO/β-CD/GCE, which are originated from the fact that the macrocyclic host β-CD can recognize the guest DA by host–guest interaction. All the above results further demonstrate the feasibility of quantitative detection DA *via* 3D-rGO/β-CD modified electrode as well.

Optimization of electrochemical detection conditions

In order to explore the reaction mechanism of DA on the electrode surface, the relationship between scanning rate (v) and peak current (i) was investigated by CV. As shown in Fig. 5a, it can be observed that the electrochemical response signal of 3D-rGO/β-CD/

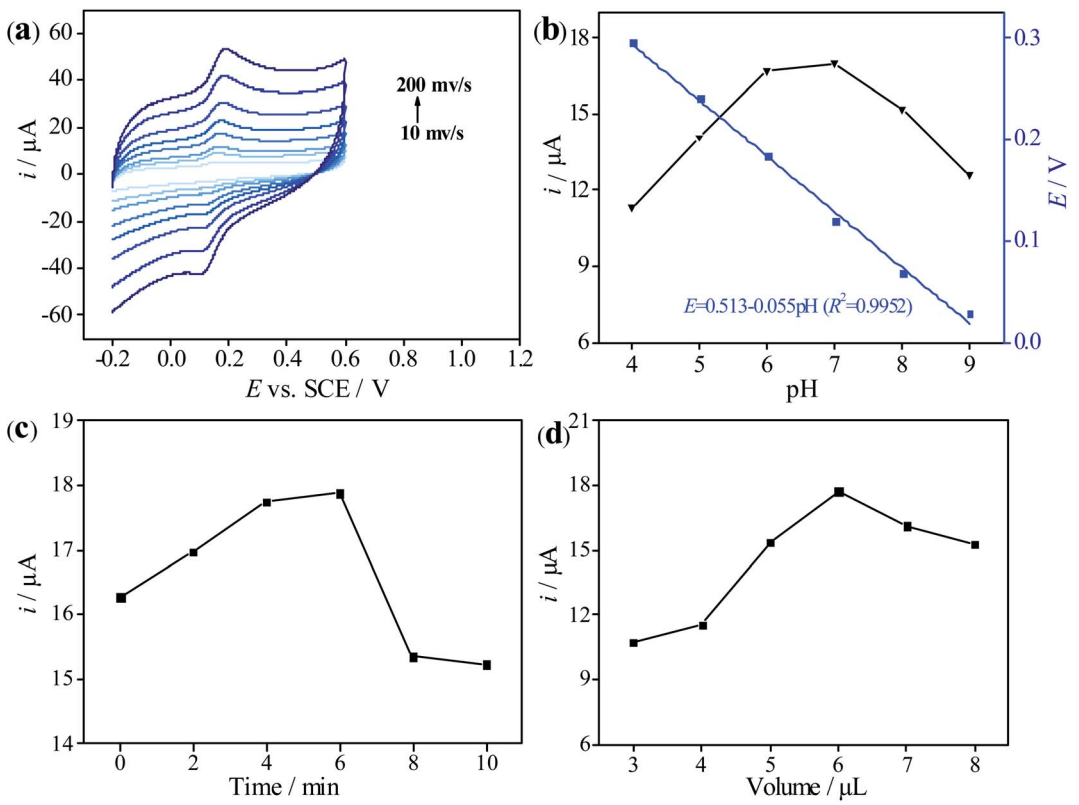

Fig. 5 (a) Cyclic voltammograms of 3D-rGO/β-CD/GCE in 0.1 M PB solution of pH 7.0 containing 50 μM DA at different scan rates from 10 to 200 mV s^{-1}. Inset: linear plot between peak currents of DA and the scan rates. (b) Influence of pH of PB on the peak current and potential for the determination towards 50 μM DA at 3D-rGO/β-CD/GCE. Influence of accumulation time (c) and volume of 3D-rGO/β-CD (2 mg mL^{-1}) (d) on detection of 50 μM DA at 3D-rGO/β-CD/GCE in 0.1 M PB of pH 7.0.

GCE towards DA increases with the increase of scanning rate. Inset of Fig. 5a illustrates the good linearity between i and v (10–200 mVs^{-1}): i_{pa} (μA) = 0.929 + 0.071v (R^2 = 0.9985) and i_{pc} (μA) = −0.533 − 0.072v (R^2 = 0.9982), respectively, which suggests that the adsorption-controlled process takes part in the reaction of DA on the 3D-rGO/β-CD/GCE. Meanwhile, the oxidation and reduction peak current of DA appear to be close, inferring that the electrochemical reaction of DA is reversible.

The pH value in the electrolyte solution plays an important role in the electrochemical detection process. The influence of different pH ranging from 4 to 9 on the electrical signal response of DA was studied by DPV. As depicted in Fig. 5b, at pH < 7, the peak current of DA increases with the increase of pH, and the peak current response of DA reaches the maximum value until pH reaches 7, indicating that this pH is most conducive to the detection of DA by 3D-rGO/β-CD/GCE. When pH > 7, the peak current decreases instead with the increase of pH. Therefore, pH = 7 is an optimal value for subsequent experiments. Additionally, the oxidation peak potential (E) decreases linearly with increasing pH values (4–9), and the corresponding linear equation is E = 0.513–0.055 pH (R^2 = 0.9952). The obtained slope of 55 mV pH^{-1} approaches to the Nernst theoretical value (58 mV pH^{-1}, 25 °C) reported in the previous literature, which proves that the electrochemical oxidation of DA is accompanied by the equal number of proton and electron transfer.[14] According to the relationship between E_p and pH, the electron transfer numbers (n) of dopamine were calculated to be 2, proving the two electrons and two proton process in the redox reaction for dopamine.

The accumulation time is considered to be an indispensable factor that affects the electrochemical sensing behavior of target molecule. As displayed in Fig. 5c, it can be clearly seen that the peak current of 3D-rGO/β-CD/GCE towards DA is highest when the accumulation time is 6 min, but it seems to be low whether the accumulation time is too long or too short, which means that the adsorption equilibrium of DA on the electrode surface is achieved at 6 min. Consequently, 6 min was employed as the appropriate time for the recognition and enrichment of DA.

Interestingly, the film thickness of the modified materials has a close relationship with the electron transfer and mass diffusion. Therefore, controlling the thickness of the sensing film is crucial, and the modification amount of 3D-rGO/β-CD dispersion on the peak current signal of DA was further examined. From Fig. 5d, it is evident that the current response augments accordingly when the coating dosage increases from 3 to 6 μL. Over 6 μL, current value decreases continuously with further increasing the modified amount, on account of the thicker film leading to blocking the electron transfer process. In view of this, 6 μL of 3D-rGO/β-CD was applied to be immobilized on the GCE surface.

Electrochemical detection of DA at 3D-rGO/β-CD/GCE

Concerning DPV reveals the higher resolution and sensitivity than CV, it is often used for quantitative analysis. Under the optimal experimental conditions, DA at different concentrations was detected by 3D-rGO/β-CD/GCE, shown in Fig. 6a. It is obvious that the oxidation peak current of DA increases with the increase of its concentration. Accordingly, two linear relationships between them are observed in the concentration range of 0.5–100 μM (Fig. 6b). For DA concentrations ranging from 0.5 to 8 μM, the linear equations is i (μA) = 0.009 + 0.296c (μM) (R^2 = 0.995) and the other is i (μA) = 1.851 + 0.103c (μM) (R^2 = 0.995) from 8 to 100 μM. At the same time, based on S/N = 3, the detection limit of DA is calculated to be 0.013 μM (ESI section S1†). Compared with other nanomaterials modified electrode previously reported in the literature (Table 1), this presented sensor proves the better result of both wide linear range and low detection limit for DA detection, opening up a new way for the high-performance measurement of DA.

Stability, repeatability and reproducibility of modified electrode

The long-term stability of 3D-rGO/β-CD/GCE was studied by detecting the electrochemical response of DA for 15 consecutive times after being storing the modified electrode under 4 °C for 30 days (Fig. S4a†). As a result, the fabricated sensor retained a response current of 95.1% of its initial current, which means there is no significant current response decay. The repeatability of the electrode was explored by repeatedly recording the

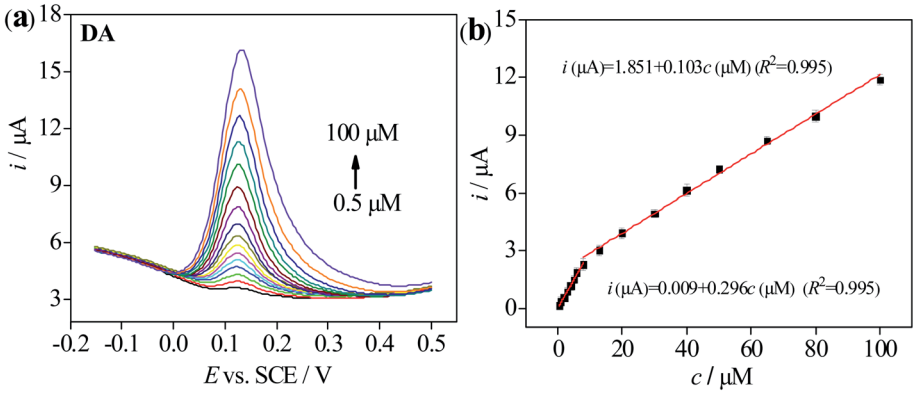

Fig. 6 (a) DPV response of 3D-rGO/β-CD/GCE with various concentration of DA in 0.1 M PB solution of pH 7.0. (b) The calibration curve of peak currents *vs.* the concentration of DA. Error bars was obtained according to the standard deviation by three independent measurements.

Table 1 Comparison of the previously fabricated similar sensors for DA determination

Electrode materials	Linear range (μM)	Detection limit (μM)	Ref.
GO	1–15	0.27	31
rGO-Co_3O_4	0–30	0.277	32
Graphene/SnO_2	0–100	1	33
AuNP/NG	0.03–48	0.01	34
GO/$TmPO_4$	2–20	0.785	35
TiO_2/graphene	5–200	2	36
3D graphene foam	0.025–25	0.025	37
3DGLCFs	0.05–10	0.01	38
β-CD/AuNPs/EDGO	0.5–120	0.024	39
Ni/NiO/C/β-CD/RGO	0.4–80	0.01	18
2HP5@GNP@WP5@g-C_3N_4	0.012–5.0	0.004	13
3D-rGO/β-CD	0.5–100	0.013	This work

electrochemical response of DA at a concentration of 20 μM for six times with the same electrode. The relative standard deviation (RSD) was found to be 3.90% (Fig. S4b†). In addition, the reproducibility of 3D-rGO/β-CD/GCE was evaluated by preparing five different modified electrodes based on the same preparation process to monitor 20 μM DA (RSD: 3.51%) (Fig. S4c†). All the experimental results demonstrated that the electrochemical analysis of DA with 3D-rGO/β-CD/GCE is not only fast, facile and cost effective but also displays good stability, repeatability and reproducibility.

Interference study

To evaluate the selectivity of the sensor, the peak current changes of DA in the presence of various interfering substances such as AA, UA, glucose, KCl and NaCl[40–42] were measured. As seen from Fig. 7a, DPV curves were recorded in PB solution of 7.0 for 1 mM AA, 100 μM 5-HT, 100 μM DA and the mixture of three compounds, which obviously showed that the peak current towards DA was much higher in contrast to AA and 5-HT. Meanwhile, no significant current signal changes were visible to the response of DA in whether individual DA or mixed solution containing 5-HT and AA besides DA. Similarly, in Fig. 7b, no appreciable variations were observed with the addition of the other interferences including 200 μM glucose, 200 μM KCl and 200 μM NaCl by chronoamperometry method. Only when a concentration of 100 μM for DA was added, a large current response change was determined, indicating that the sensor has high selectivity for the determination of DA molecules being free from the interference from the other substances.

In addition, the interference studies have been also performed on the bare GCE and 3D-rGO/GCE except for 3D-rGO/β-CD/GCE (Fig. S5†). It is found that no obvious interference exists from AA and the other interferences (glucose, KCl and NaCl) towards DA for bare GCE and 3D-rGO/GCE except 5-HT. Nevertheless, in Fig S5a and c,† in spite of the peaks for DA and 5-HT appeared at bare GCE and 3D-rGO/GCE (blue line), a somewhat overlapping peak of these two biomolecules is obviously visible in the DPV responses of bare GCE and 3D-rGO/GCE, thus 5-HT may exert a certain influence to the detection of DA due to its presence in some cases. Compared to bare/GCE and 3D-rGO/GCE, it is very apparent that the distinctly distinguishable peaks for DA and 5-HT shown in Fig. 7a, further revealing the better selectivity towards DA at 3D-rGO/β-CD/GCE. It is clear to suggest that β-CD is great for improving selectivity of DA. Moreover, it has been proved that there exists 5-HT in human serum,[1,2,10] when 3D-rGO/β-CD modified electrode is applied in practical serum sample, dopamine detection and recovery experiments will not be affected by 5-HT *via* the

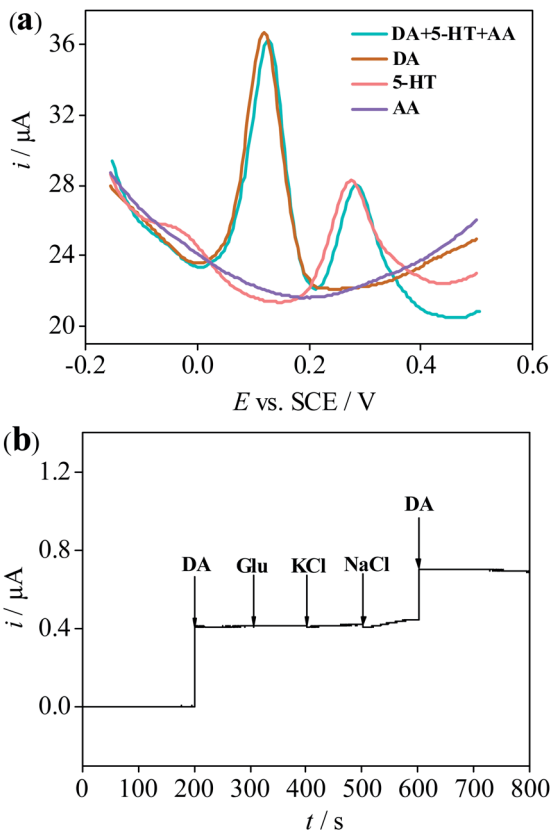

Fig. 7 (a) DPV responses of 3D-rGO/β-CD/GCE in 0.1 M PBS (pH = 7.0) for 1 mM AA, 100 μM DA, 100 μM 5-HT and the mixture of 1 mM AA, 100 μM DA and100 μM 5-HT. (b) Amperometric responses of the 3D-rGO/β-CD/GCE for the addition of 100 μM DA and 200 μM glucose, 200 μM KCl and 200 μM NaCl in 0.1 M PBS (pH = 7.0).

standard adding method. In addition, the peak current values of DA with the same concentration at various electrodes also make the differences in Fig. 7a and S5.† Compared to the both bare/GCE and 3D-rGO/GCE, the higher current response of DA whether in the DPV measurements and in the chronoamperometry experiments and more easily distinguishable peak potentials of DA towards other interference substances at 3D-rGO/β-CD/GCE, further providing additional support that the β-CD is what is facilitating DA electrochemical sensitivity and selectivity.

Sample analysis

To determine the accuracy and the application potential, the 3D-rGO/β-CD/GCE was employed for the detection of DA concentration in human serum and urine *via* the standard adding method. Before determination, the serum and urine samples were diluted 5 times and 2-fold with 0.1 M PB solution, respectively. The DA in the diluted serum failed to be found under the experimental conditions by DPV, which agrees with the results of published paper.[14,43,44] Whereas DA in the diluted urine was determined as 0.72 μM, meaning the 1.44 μM for concentration of DA in the pristine urine, which accords with the normal range value from 0.3 to 3.13 μM under healthy physiological conditions.[45] Then, for performing the spiking experiment, a certain amount of DA was added into the diluted serum and urine, next further mixed to obtain different concentrations of DA. After a period of reaction time, the DPV signal of DA in the solution was detected. The concentrations of DA were calculated from the calibration curves given in Fig. 6. From the corresponding results listed in Table S1,† it is seen that the measured concentrations approached to the added values, then the recoveries were about 99.40–102.4% and 98.8–101.7%, RSD values were below 2.63% and below 3.39% in the diluted serum and urine, respectively. The above data reveal that great satisfactory, reliability and the practical utilization in real sample analysis.

Stoichiometry and association constants of β-CD and DA

UV-visible spectroscopy measurements were applied to explore the stoichiometry of the inclusion complex both β-CD and DA, further providing a strong evidence for the detection of DA molecule. Fig. 8 reveals the absence and presence of various concentrations of β-CD ranging from 0.5 to 10 mM. From Fig. 8a, we can notice a maximum absorption of DA appearing at 280 nm in the UV region, meanwhile the absorbance intensity gradually gives rise to enhancing with the concentration increase of β-CD, demonstrating that DA was included within the cavity of the β-CD and forms the host–guest inclusion complex (β-CD-DA). On the basis of eqn (1), it is clear that the linear relationship of double reciprocal plot can be obtained when n value is 1, meaning a 1 : 1 stoichiometric ratio in the complexation process of the inclusion complex (Fig. 8b).

$$\frac{1}{A - A_0} = \frac{1}{\Delta\varepsilon \times [\text{DA}]} + \frac{1}{\Delta\varepsilon \times [\text{DA}] \times K \times [\beta\text{-CD}]_0^n} \quad (1)$$

The association constant for β-CD against DA was evaluated using the relationship proposed by Benesi *et al.* in eqn (1),[46]

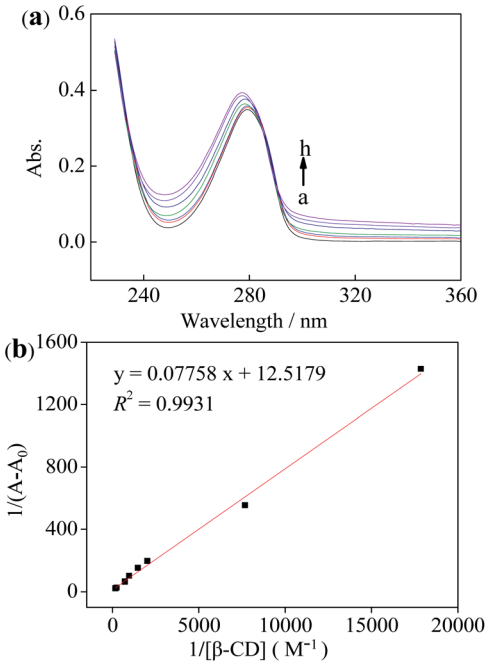

Fig. 8 (a) UV-visible spectroscopy the absence (a) and presence of various concentrations of β-CD (b–h corresponding to 0.5, 1, 2, 3, 4, 5, 6, 7, 8, 9 and 10 mM, respectively). (b) Double reciprocal plots for β-CD combing DA under the varying concentrations β-CD.

where A and A_0 are the absorption intensities of the β-CD–DA complex and independent DA guest, respectively, and K is the association constant of complex. Besides, $[\beta\text{-CD}]_0^n$ and [DA] respectively stand for the initial concentrations of β-CD and DA, and $\Delta\varepsilon$ represents the differential molar extinction coefficients the complex β-CD–DA and guest DA. From the ratio of the intercepts towards the slopes, K value of 161.4 M^{-1} was computed, verifying a perceptible inclusion interaction.

Conclusions

In conclusion, a simple preparation method of three-dimensional reduced graphene oxide composite modified by cyclodextrin is proposed. It was modified on GCE to prepare a new sensor for electrochemical detection of DA. The modified electrode has high electrochemical performance because of its large specific surface area, good water solubility, high conductivity and excellent catalytic activity. By detecting the electrochemical behavior of DA with DPV, a wider linear range and a lower detection limit were obtained, which showed the characteristics of high sensitivity and small interference. The sensor based on the preparation shows great potential in DA detection. This method can provide a new idea in electrochemical sensor detection.

Compliance with ethical standards

All experiments were performed in accordance with the Guidelines "Measures for the Ethical Review of Biomedical Research Involving Humans" and the "Management Regulations for Human Biological Samples" issued by the National

Health Commission of the People's Republic of Experiments were approved by the ethics committee at Shanxi Medical University. Informed consents were obtained from human participants of this study.

Conflicts of interest

There are no conflicts to declare.

Acknowledgements

This work was financially supported by the National Natural Science Foundation of China (No. 21976113), the Natural Science Foundation of Shanxi Province (No. 201801D221059).

References

1 Y. P. Huang, Y. E. Miao, S. S. Ji, W. W. Tjiu and T. X. Liu, *ACS Appl. Mater. Interfaces*, 2014, **6**, 12449–12456.
2 J. D. Berke, *Nat. Neurosci.*, 2018, **21**, 787–793.
3 Y. L. Zhang, S. J. Qi, Z. G. Liu, Y. P. Shi, W. Q. Yue and C. Q. Yi, *Mater. Sci. Eng., C*, 2016, **61**, 207–213.
4 R. M. Wightman, L. J. May and A. C. Michae, *Anal. Chem.*, 1988, **60**, 769A–779A.
5 Y. Y. Zhou, C. Liu, H. P. Yu, H. W. Xu, Q. Lu and L. Wang, *Spectrosc. Lett.*, 2006, **39**, 409–420.
6 F. Huang, J. Li, H. L. Shi, T. T. Wang, W. Muhtar, M. Du, B. B. Zhang, H. Wu, L. Yang, Z. B. Hu and X. J. Wu, *J. Neurosci. Methods*, 2014, **229**, 8–14.
7 M. E. P. Hows, L. Lacroix, C. Heidbreder, A. J. Organ and A. J. Shah, *J. Neurosci. Methods*, 2004, **138**, 123–132.
8 X. J. Sun, L. Zhang, X. H. Zhang, X. X. Liu, J. Jian, D. C. Kong, D. C. Zeng, H. M. Yuan and S. H. Feng, *Biosens. Bioelectron.*, 2020, **153**, 112045.
9 Q. T. Huang, X. F. Lin, L. L. Tong and Q. X. Tong, *ACS Sustainable Chem. Eng.*, 2020, **8**, 1644–1650.
10 W. T. Liang, Y. Q. Rong, L. F. Fan, C. H. Zhang, W. J. Dong, J. Li, J. P. Niu, C. Yang, S. M. Shuang, C. Dong and W. Y. Wong, *Microchim. Acta*, 2019, **186**, 751.
11 S. K. Arumugasamy, S. Govindaraju and K. Yun, *Appl. Surf. Sci.*, 2020, **508**, 145294.
12 G. Xu, Z. Jarjes, V. Desprez, P. Kilmartin and J. Travas-Sejdic, *Biosens. Bioelectron.*, 2018, **107**, 184–191.
13 X. P. Tan, S. H. He, X. Liu, G. F. Zhao, T. Huang and L. Yang, *Microchim. Acta*, 2019, **186**, 703.
14 R. Y. Li, T. T. Yang, Z. J. Li, Z. G. Gu, G. L. Wang and J. K Liu, *Anal. Chim. Acta*, 2017, **954**, 43–51.
15 E. Fazio, S. Spadaro, M. Bonsignore, M. Bonsignore, N. Lavanya, C. Sekar, S. G. Leonardi, G. Neri and F. Neri, *J. Electroanal. Chem.*, 2018, **814**, 91–96.
16 R. Zhang and W. Chen, *Biosens. Bioelectron.*, 2017, **89**, 249–268.
17 P. Makvandi, M. Ghomi, M. Ashrafizadeh, A. Tafazoli, T. Agarwal, M. Delfi, J. Akhtari, E. N. Zare, V. V. Padil and A. Zarrabi, *Carbohydr. Polym.*, 2020, **250**, 116952.
18 X. Q. Cui, D. Cao, R. Djellabi, M. Qiao, Y. Wang, S. Zhao, R. Mao, Y. Gong, X. Zhao and B. Yang, *J. Electroanal. Chem.*, 2019, **851**, 113407.
19 X. Q. Cui, B. Yang, S. Zhao, X. W. Li, M. Qiao, R. Mao, Y. Wang and X. Zhao, *Sens. Actuators, B*, 2020, **315**, 128091.
20 O. J. Kingsford, J. J. Qian, D. P. Zhang, Y. H. Yi and G. B. Zhu, *Anal. Methods*, 2018, **10**, 5372–5379.
21 A. Heydariaband and H. Sheibani, *RSC Adv.*, 2016, **6**, 9760–9771.
22 B. Mirzaei, A. Zarrabi, A. Noorbakhsh, A. Amini and P. Makvandi, *RSC Adv.*, 2021, **11**, 7862.
23 W. T. Liang, Y. Q. Rong, L. F. Fan, W. J. Dong, Q. C. Dong, C. Yang, Z. H. Zhong, C. Dong, S. M. Shuang and W. Y. Wong, *J. Mater. Chem. C*, 2018, **6**, 12822–12829.
24 Y. Q. Rong, Y. Huang, P. Y. Jin, C. Yang, Z. H. Zhong, C. Dong and W. T. Liang, *J. Water Process. Eng.*, 2020, **37**, 10134.
25 B. Tang, G. J. Ji, Z. W. Wang, H. Q. Chen, X. F. Li, H. G. Yu, S. Li and H. Liu, *RSC Adv.*, 2017, **7**, 45280–45286.
26 Z. X. Hou, L. X. Kong, S. N. Zou, L. W. Zhao and L. R. Yang, *RSC Adv.*, 2020, **10**, 2989–2997.
27 Z. G. Liu, Q. Xue and Y. J. Guo, *Biosens. Bioelectron.*, 2017, **89**, 444–452.
28 Y. Liu, S. B. Huang, X. S. Zhao and Y. Q. Zhang, *Colloids Surf., A*, 2018, **539**, 1–10.
29 G. J. Rani, K. J. Babu, G. G. kumar and M. A. J. Rajan, *J. Alloys Compd.*, 2016, **688**, 500–512.
30 Y. L. Huang, Y. Tan, C. Q. Feng, S. Q. Wang, H. M. Wu and G. X. Zhang, *Microchim. Acta*, 2019, **186**, 10.
31 F. Gao, X. Cai, X. Wang, C. Gao, S. Liu, F. Gao and Q. Wang, *Sens. Actuators, B*, 2013, **186**, 380–387.
32 A. Numan, M. M. Shahid, F. S. Omar, K. Ramesh and S. Ramesh, *Sens. Actuators, B*, 2017, **238**, 1043–1051.
33 R. Nurzulaikha, H. N. Lim, I. Harrison, S. S. Lim, A. Pandikumar, N. M. Huang, S. P. Lim, G. S. H. Thien, N. Yusoff and I. Ibrahim, *Sens. Bio-Sens. Res.*, 2015, **5**, 42–49.
34 T. D. Thanh, J. Balamurugan, S. H. Lee, N. H. Kim and J. H. Lee, *Biosens. Bioelectron.*, 2016, **81**, 259–267.
35 H. P. Huang, Y. F. Yue, Z. Z. Chen, Y. N. Chen, S. Z. Wu, J. S. Liao, S. J. Liu and H. R. Wen, *Microchim. Acta*, 2019, **186**, 89.
36 Y. Fan, H. T. Lu, J. H. Liu, C. P. Yang, Q. S. Jing, Y. X. Zhang, X. K. Yang and K. J. Huang, *Colloids Surf., B*, 2011, **83**, 78.
37 X. C. Dong, X. W. Wang, L. H. Wang, H. Song, H. Zhang, W. Huang and P. Chen, *ACS Appl. Mater. Interfaces*, 2012, **4**, 3129–3133.
38 W. F. Deng, X. Y. Yuan, Y. M. Tan, M. Ma and Q. J. Xie, *Biosens. Bioelectron.*, 2016, **85**, 618–624.
39 Z. Chang, Y. L. Zhou, L. J. Hao, Y. Q. Hao, X. Zhu and M. T. Xu, *Anal. Methods*, 2017, **9**, 664–671.
40 Y. Fu, H. Yang and J. Guo, *IEEE Trans. Biomed. Circuits Syst.*, 2019, **15**, 6389–6394.
41 J. Guo, *Anal. Chem.*, 2016, **88**, 11986–11989.
42 J. Guo and X. Ma, *Biosens. Bioelectron.*, 2017, **94**, 415–419.
43 W. F. Deng, X. Y. Yuan, Y. M. Tan, M. Ma and Q. J. Xie, *Biosens. Bioelectron.*, 2016, **85**, 618–624.
44 S. Daemi, A. A. Ashkarran, A. Bahari and S. Ghasemi, *J. Colloid Interface Sci.*, 2017, **494**, 290–299.
45 S. Dalirirad and A. J. Steckl, *Anal. Biochem.*, 2020, **596**, 113637.
46 H. A. Benesi and J. H. Hildebrand, *J. Am. Chem. Soc.*, 1949, **71**, 2703–2707.